LA-7087-MS
Informal Report

Special Distribution

Seismic Investigation of the Nuclear Fuel Services, Inc., Reprocessing Plant at West Valley, New York

Issued: March 1978

los alamos
scientific laboratory
of the University of California
LOS ALAMOS, NEW MEXICO 87545

UNITED STATES
DEPARTMENT OF ENERGY
CONTRACT W-7405-ENG. 36

LA-7087-MS
Informal Report
Special Distribution

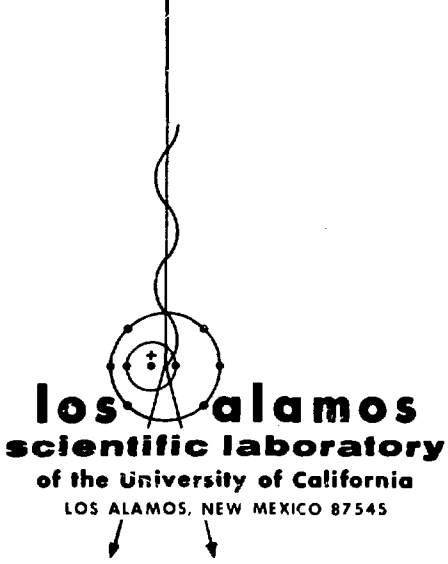

Seismic Investigation of the Nuclear Fuel Services, Inc., Reprocessing Plant at West Valley, New York

Elton G. Endebrock
Robert J. Bartholomew
Joel G. Bennett
Robert I. Brasier*
William F. Corcoran

*Los Alamos Technical Associates, P.O. Box 410, Los Alamos, NM 87544

Manuscript completed: March 1978
Issued: March 1978

Prepared for the US Nuclear Regulatory Commission
Office of Nuclear Regulatory Research

CONTENTS

SEISMIC INVESTIGATION OF THE NUCLEAR FUEL SERVICES, INC., REPROCESSING PLANT AT WEST VALLEY, NEW YORK

by

Elton G. Endebrock
Robert J. Bartholomew
Joel G. Bennett
Robert I. Brasier
William F. Corcoran

ABSTRACT

An investigation was undertaken to determine the earthquake level at which the Nuclear Fuel Service, Inc., Reprocessing Plant at West Valley, New York, could first experience a predefined structural failure. The effort was divided into tasks of evaluating soil-structure interaction, determining overall facility motion, and analyzing the substructures. The analysis included using two- and three-dimensional finite element computer codes. Shear wall failure, cell flexural failure (beam action), and foundation (pile) failure were identified as possible structural failure types. The cells that contain radioactive materials and that are required to confine such materials during an earthquake should remain intact up to 0.20 g's. At the same loading, the piles supporting the confinement cells could undergo displacements sufficient to cause fracture of piping between nonmonolithically connected cells.

I. INTRODUCTION

A. Task

The Los Alamos Scientific Laboratory (LASL) and the Lawrence Livermore Laboratory (LLL) were asked to perform seismic evaluations of the Nuclear Fuel Services, Inc., (NFS) reprocessing facility located at West Valley, New York. This request by the Fuel Reprocessing and Recycle Branch of the Nuclear Regulatory Commission (NRC) resulted from an application by NFS for a license to modify and operate the West Valley Facility. The procedures and results of LASL's investigations are presented in this report.

When the NFS facility was designed and constructed, no specific seismic standards for nuclear fuel reprocessing facilities existed; hence, it was designed to Uniform Building Code (UBC) requirements. Because of problems with the application of these seismic criteria to an existing facility, LASL and LLL were asked to undertake a seismic-structural analysis of the facility. The primary task was to determine the smallest earthquake that could produce the onset of failure in the weakest structural element. Because structures are difficult to analyze against such qualitative criteria, the failure criteria were further interpreted so that they would be meaningful to structural analysis. NFS and its consultants provided the information necessary for conducting the seismic evaluation.

B. Background Information

The NFS reprocessing facility was constructed in 1964, and reprocessing of spent fuel started in April 1966. It was shut down early in 1972 for modifications and has been used only for storage since then.

The facility includes thick-walled reinforced concrete cells that surround the reprocessing lines, and rooms and hallways that are divided by concrete block walls and structural steel framing. The rooms and hallways are located between, on top of, or adjacent to the massive concrete walls. Those enclosed by the block walls are used for access, offices, personnel space, chemical storage, instrumentation, and other functions.

The seismic evaluation included only that part of the facility that provides confinement to the reprocessing line. The cells whose failure might cause or substantially contribute to the release of radioactivity approaching the 10 CFR 100 guidelines are listed below:

- GPC - General Purpose Cell
- PMC - Process Mechanical Cell
- CPC - Chemical Process Cell
- LWC - Liquid Waste Cell
- XPC - Extraction and Product Purification Cells
- AGC - Acid and Off-Gas Recovery Cell
- UPC - Uranium Product Cell
- EDR - Equipment Decontamination Room
- SRC - Scrap Recovery Cell
- AC - Analytical Cells
- VWR - Ventilation Wash Room
- MCR - Mechanical Crane Room

The aggregate of these cells is referred to as the confinement structure.

The cell walls are reinforced concrete with thicknesses from 0.3 to 1.5 m (1 to 5 ft) and heights to 18.3 m (60 ft). Wall and roof thicknesses were based on radiation protection requirements and not on strength requirements; consequently, the amount of reinforcing steel in the walls is relatively small.

There are many ways to define failure. For the seismic evaluation of the NFS facility, failure was presumed to occur when the calculated seismic loads equaled the ultimate strength of a structural element in the confinement structure. The failure computations were done according to the procedures outlined in the American Concrete Institute (ACI) Building Code,[1] but with all load and capacity reduction factors taken as unity.

C. General Analysis

The seismic evaluation of the NFS confinement structure was divided into three tasks: (1) investigation of soil-structure interaction, (2) determination of overall motion of the structure, and (3) analysis of substructures.

The soil-structure system was modeled, and site-dependent response spectra at the foundation level were developed. These spectra were then used to obtain the response of a three-dimensional fixed-base finite element model of the confinement structure by the use of model superposition. These acceleration responses were used to obtain the inertial forces from which moments and shears were obtained within substructures. Then substructure seismic loads were compared to the corresponding calculated ultimate loads.

II. SOIL-STRUCTURE INTERACTION

A. Introduction

Existing and available analytical tools were used whenever possible. The nonproprietary code LUSH,[2] a two-dimensional finite element code for the complex response analysis of soil-structure systems, was selected for the soil-structure interaction investigations. The soil-structure model used in LUSH consists of plane-strain triangular or quadrilateral elements. LUSH approximates the nonlinear effects that occur in soil masses subjected to earthquake motions by the equivalent linear method. The model is excited by a specified acceleration time history at the base, which does not have to be horizontal, and the specified motion can have any direction in the model plane.

Neither site-dependent design response spectra or acceleration time histories were available for describing the earthquake characteristics, so the NRC Design Response Spectra were selected as the basis for the free-field earthquake motion.[3] For input, LUSH requires an acceleration time history at the base of the soil-structure model. Therefore, it became necessary to generate artificial acceleration time histories that were compatible with the NRC Design Response Spectra and then to transform these generated histories to compatible bedrock level histories.

Three artificial acceleration time histories in orthogonal directions were generated through the use of a modified version of the code SIMEAR,[4] and the code SHAKE was used to obtain the bedrock level acceleration time histories.[5]

The sequence of events for the soil-structure interaction investigations is summarized below.

1. Generate artificial earthquake acceleration time histories that are compatible with the NRC Design Response Spectra.

2. Generate bedrock acceleration time histories that are consistent with the foundation level artificial acceleration time histories.

3. Use the bedrock acceleration time histories in LUSH to determine the soil-structure interaction effects.

B. Generation of Artificial Acceleration Time Histories

Regulatory Guide 1.60 recommends that the response spectra of the generated earthquake acceleration time histories approximately envelop the NRC Design Response Spectra.[3] The response spectra were developed using 7% damping as recommended in Regulatory Guide 1.61 for reinforced concrete and the design basis earthquake.[6]

The generated earthquake acceleration time histories for the horizontal and vertical directions were obtained through the use of a modified version of SIMEAR.[4] SIMEAR was written as a single-pass program that uses a Fourier spectrum input. The original SIMEAR did not yield an earthquake acceleration record that satisfactorily enveloped the specified response spectrum, so iteration capabilities were incorporated in the program.[7] After modification, an earthquake acceleration time history could be generated that would envelop a specified response spectrum to any degree of desired accuracy by a proper selection of the number of iterations.

Three artificial earthquake acceleration time records were generated for this investigation, two horizontal and one vertical. One of the horizontal records is shown in Fig. 1. A comparison of its response spectrum to the NRC Design Response Spectrum is shown in Fig. 2. The largest deviation below the NRC Spectrum was less than 9% at a frequency of 18 Hz.

C. Determination of Bedrock Motions

A deconvolution analysis was necessary to obtain the bedrock motions that would have to exist to produce the specified motions at the selected free-field level. These motions were generated through the use of SHAKE. SHAKE is based on the one-dimensional wave propagation theory and computes the responses in a system of homogeneous, viscoelastic layers of infinite horizontal extent subjected to vertical shear waves that produce only horizontal displacements. SHAKE incorporated strain-dependent damping and shear moduli of the soil layers. Bedrock acceleration time histories were generated for surface acceleration record magnitudes of 0.06, 0.12, and 0.18 g's.

The soil layers under the facility increase in depth from west to east, the bedrock slope being approximately 1/8.6. SHAKE was used to obtain the bedrock acceleration records even though the assumption of horizontal soil layers was not satisfied. The soil-layering characteristics at the midpoint of the E-W soil-structure model were used to determine the input information for SHAKE. The application of SHAKE to this problem will not result in significant differences in the frequency characteristics of the motions, but could change the amplitude responses.[8]

Vertical bedrock motions were also generated using SHAKE, except that the shear moduli values for G were replaced by the values $2G(1 - \nu)/(1 - 2\nu)$,[9] where ν is Poisson's ratio. As will be seen later, the use of vertical design response spectra generated in this manner resulted in larger structural responses than would have been obtained had the usual procedure of the use of vertical response spectra as two-thirds of the horizontal design response spectra been followed. Two-thirds of the horizontal response spectra was not used because this relationship has not been demonstrated to be valid for earthquakes in the eastern part of the United States.

D. Site Subsurface Conditions

The soil deposits at the facility are mostly unsorted, unstratified, irregular, and discontinuous glacial deposits. Three different

horizons of glacial till were distinguished within the soil deposit overlaying the bedrock. The material in the lower layer is a dense to very dense mixture of sand, gravel, silt, and clay. The intermediate layer is a medium stiff and highly plastic silty clay that contains some sand and gravel. The top layer is composed of medium firm to firm silty clay with some gravel. This upper layer is approximately 6.1 m (20 ft) thick.

Groundwater was encountered at depths of 1.2 to 1.8 m (4 to 6 ft) below the ground surface, and the soil below this level is saturated. The upper and lower soil layers are mostly free draining, but the intermediate layer is impervious. In addition, the water level in the bore holes varied depending upon their depth. Water wells cannot be used for a dependable water supply in this area. All of these observations suggest that this is a perched water table and not the static water table level. The static water table has not been specifically located but is believed to be at a depth of approximately 23 m (75 ft).[10,11]

The dense lower layer and the firm upper layer, coupled with their free-draining characteristics, preclude the possibility of soil liquification at the facility for the projected earthquake intensities.

The process building rests on piles that were driven to refusal into the dense lower soil layer. A pile foundation was selected to span the highly compressible intermediate layer, thereby greatly reducing settlements. No significant settlements have been observed since the completion of the facility.

Bore hole logs and subsurface profile maps were provided by NFS. The soil-structure models were constructed from this information and from the facility construction drawings. The soil layers were idealized to obtain a more uniform layering than was evident from the data.

E. Modeling of the Soil-Structure System

1. Introduction. The NFS confinement structure has several thick-walled reinforced concrete cells, some monolithically connected and others simply located adjacent to one another. The cells form an asymmetric structure as illustrated in Fig. 3. Some cells are buried, and some have foundations near grade level. The facility cross section changes dramatically from point to point; hence, it does not have ideal characteristics for a plane-strain analysis. Nevertheless, the limitations of LUSH dictated that the confinement structure be modeled as a two-dimensional structure. Asymmetrical structures would be more subject to torsional action than symmetrical structures; however, the LUSH two-dimensional soil-structure models do not allow for torsional effects.

The piles supporting the facility are located mostly under the cell walls. The large number of piles (465) and the two-dimensional representation of the confinement structure made it impossible to consider individual piles in the soil-structure models. A literature search failed to find procedures or methods for two-dimensional modeling of piles supporting a three-dimensional structure; hence, in constructing the soil-structure models, certain assumptions were made. These assumptions and their effect upon the final results of the analysis will be discussed later.

The modeling of the soil-structure system required modeling of the confinement structures, the soil deposits, and the pile foundation. The modeling procedures and methods are described below.

2. Two-Dimensional Modeling of the Facility. The NFS reprocessing confinement structure was described earlier. The confinement structure's long and short dimensions coincide with N-S and E-W, so the global reference axes for the models were selected for these directions.

A wood model of the confinement part of the facility was constructed for use as a visual aid because the facility is so complicated. The model provides an immediate visual assessment of the relative sizes of the individual cells and their locations. Several views of the model are shown in Figs. 3 through 5.

Soil-structure models were constructed for the N-S and E-W directions. The two-dimensional shapes of the facility were obtained by taking its profiles. For example, the N-S structure profile was obtained from a view of the facility from the east, and the E-W structure profile was obtained

from a view from the north. The structure profiles were idealized in that small appendages were disregarded. The model dimensions used were 54.9 m (180 ft) N-S and 43.3 m (142 ft) E-W direction.

Density and shear modulus values of the facility structure were required as input to LUSH. The density for the N-S model was obtained by dividing the total weight of the reprocessing facility plus the estimated weight of the Fuel Receiving and Storage Pool (FRS) by the length of the facility in the E-W direction and then dividing by the area of the facility projected in the N-S direction. The density for the E-W model was computed in a similar manner. Note that this technique does not yield the same densities for the two models. The FRS was not included in the seismic analysis of the facility, but the FRS is located adjacent to the reprocessing plant and therefore influences the soil-structure interaction. Hence, the FRS weight was included in the soil-structure investigations.

The shear modulus was estimated by first selecting several confinement cells whose wall thicknesses ranged from the thinnest to the thickest. The ratio of the wall cross-sectional areas to the total cross-sectional area was computed for each of the selected confinement cells. Average ratios were determined and adjusted to account for the difference in form factors between the model area shape and the actual cell shapes. The shear stiffness of the model was equated to the estimated shear stiffness of the facility. The equivalent shear modulus of the model was then computed. Sample calculations are presented in Appendix A. The same shear modulus was used in both soil-structure models. Damping in the structural model was taken as 2%.

3. Modeling of the Soil Deposits. The soil deposit models for the N-S and E-W directions were constructed from information provided by NFS.[10,11] The soil layers and bedrock surface were idealized to obtain more uniform boundaries. The dimensions of the elements were based on the dimensions of the models and the recommendations in the LUSH users' manual.[2] The soil model extensions beyond the facility models were also based upon recommendations in the users' manual. Compromises between the fineness or coarseness of the finite element mesh and the capacity of the computer were necessary. The finite element meshes for the two soil-structure models are shown in Figs. 6 and 7. The side boundary nodal points were restrained to horizontal motions for horizontal acceleration time history inputs and to vertical motions for vertical acceleration time history inputs.

4. Modeling of the Piles. The pile modeling from a three-dimensional arrangement to a two-dimensional model was perplexing. No guidelines were available from publications, so the procedures described below were developed by the authors.

Storage and time constraints imposed by the computer system limited each soil-structure model to four lumped piles. Their locations were selected based on the structure profiles at the soil-structure interface. A lumped pile was located at both ends of the profiles with the two intermediate lumped piles located so that the underground cell (GPC) was supported by at least one lumped pile. The locations of the lumped piles with respect to the structure foundation profiles are shown in Figs. 8 and 9. The plan view of the confinement structure foundation was then sectioned in the N-S and E-W directions. The number of piles in each section was counted. Pile distribution patterns were determined for the confinement structure in both directions as shown in Figs. 8 and 9. The pile distribution graphs were sectioned according to the location of the lumped piles. The number of individual piles in each section (1 through 4) was determined and assigned to the corresponding lumped pile. These values are also indicated in Figs. 8 and 9. The width of the lumped piles was based on the number of individual piles assigned to them and the visually estimated fraction of the structure foundation supported by each lumped pile.

Once the piles were modeled, equivalent material properties were obtained for input into LUSH. The piles assigned to a lumped pile were nearly equal with respect to the orientation of the principal inertia axes (N-S or E-W) of the

pile sections. The total moments of inertia and areas of the actual piles were obtained and summed for each lumped pile. For horizontal motions, the flexural stiffness (EI) of the actual piles was equated to the EI of the lumped pile in each section. The moments of inertia of the lumped piles were obtained from their dimensions. The procedure for computing the lumped pile moduli of elasticity was the same for the two soil-structure models. For vertical motions the axial stiffness (EA) of the actual piles was equated to the EA of the lumped piles in each section. Different pile properties were necessary for vertical and horizontal motions. The ratio of modulus of elasticity to cross-sectional area for a rectangular section as used in the models was not the same as the pile H-sections. The estimated equivalent stiffness values are given in Table I, and the sample calculations are presented in Appendix A. Steel density and 2% damping were used for all lumped piles.

The procedures used to model the piles will capture the gross effects caused by unidirectional motion, which is the primary goal. Local effects caused by spacing and location of individual piles could not be determined.

F. Discussion of Results

The soil-structure interaction analysis was performed to develop the foundation level response spectra necessary for the dynamic analysis of the NFS confinement structure. The material properties used for the structure and piles were determined as described in the preceding sections, and the soil-layer properties were representative of the site. These properties are illustrated in Fig. 10 and listed in Table II. The water table was assumed to be 22.9 m (75 ft) below ground.

The soil and foundations are probably not fully in contact. Although the soil could have settled, there has been no settlement of the pile-supported facility. Compensation for the loss of friction between the soil and foundation was accomplished by assigning relatively low shear moduli [low strain values of 4.8 MPa (100 kip per square foot)] to the soil elements in contact with the foundation. Only the shear moduli of the soil elements in contact with vertical surfaces of the facility were not reduced. This resulted in larger lateral forces on the piles.

Acceleration time histories at specified nodal points within the model were computed by LUSH using the bedrock level acceleration time histories computed by SHAKE as input. Response spectra were then obtained from the nodal acceleration time histories. Nodal response spectra were generated at four points along the bottom of the facility foundation for both soil-structure models. The selected nodal points are indicated in Figs. 6 and 7 by enlarged points. Response spectra were developed for the horizontal and vertical directions for both soil-structure models. The response spectra for these cases at 7% damping are shown in Figs. 11 through 18.

The response spectra at different nodal points along the foundation are not identical in magnitude or shape. The use of SAP IV (see section III.A) to determine the dynamic response of the facility constrains one to the use of a single response spectrum shape for each calculation. Unfortunately, the horizontal and vertical response spectra were so different that they could not be combined into a single shape; hence, one response spectrum was obtained for the two horizontal directions, and another response spectrum was obtained for the vertical direction.

A single horizontal response spectrum for the foundation can be obtained by averaging the individual nodal responses or by enveloping the individual nodal response spectra. The same can be done for the vertical direction. The foundation level response spectra were envelopes of the nodal response spectra because this would produce larger structural responses. The horizontal and vertical spectra are shown in Figs. 19 and 20.

The maximum vertical responses of 1.8 g's and 3.0 g's for the free-field earthquake accelerations of 0.12 g's and 0.18 g's, respectively, appear unusually large (Fig. 20). Table III shows that the maximum responses in Case I are significantly lower than in Case II and that they occur at different frequencies. This indicates that the large responses in Case II result from a resonant or near resonant condition. The significance is that soil amplification at the site may be severe.

LUSH is not well suited for investigating the effects of different soil properties on the response of the soil-structure system. It does not adjust the soil stresses for pore water pressure, and the material properties must be input for each individual element. A new set of element data cards must be generated for each change in input values, so for models that contain a large number of elements, the effort involved can be considerable. Therefore, only one set of input parameters was used.

The effect of the pile stiffness on the foundation level response spectra was investigated. The N-S soil-structure model was used with motions applied in the horizontal direction. Response spectra for stiff, average, and no piles are shown in Fig. 21. The maximum response occurs at about the same frequency; however, for frequencies above 10 Hz, the response spectra differ little. This is the frequency range of primary importance to the structure.

Displacements of selected nodal points were also part of the output from LUSH and were used in the investigation of the pile forces to be described later.

III. SEISMIC ANALYSIS OF THE NFS CONFINEMENT STRUCTURE

A. Introduction

The purpose of this investigation was to evaluate the response of the NFS Plutonium Fuel Recycle Plant to a seismic event. A fixed-base three-dimensional finite element model of the confinement structure was established. The seismic response of this model was obtained with the computer code SAP IV.[12] This code has many of the capabilities needed in analyzing a three-dimensional structure subjected to seismic loading and is relatively easy for the user to modify.

The dynamic responses were obtained by combining the responses of individual modes in a response spectrum modal analysis. If we define $S_d(\omega)$ as the displacement response spectrum that is the envelope of all maximum responses that a single degree-of-freedom system has to all ground motions of a given magnitude, then the maximum modal response $\{U_i\}$ for the ith mode is given by

$$\{U_i\} = \{\phi_i\}\left[\{\phi_i\}^T \{M_i\}\right] S_{dx}(\omega_i) + \{\phi_i\}\left[\{\phi_i\}^T \{M_i\}\right] S_{dy}(\omega_i) + \{\phi_i\}\left[\{\phi_i\}^T \{M_i\}\right] S_{dz}(\omega_i) \quad . \qquad (1)$$

The expression $\{\phi_i\}^T \{M_i\}$ is defined as the participation factor, and the contribution to $\{M_i\}$ (mass matrix) is replaced with zero if a node has no defined degree of freedom in the direction being considered. The term $\{\phi_i\}$ is the eigenvector for the ith mode. In writing Eq.(1), the ground acceleration vector can be written as the sum of three components in the x-, y-, and z-directions, and $S_{dx}(\omega_i)$, $S_{dy}(\omega_i)$, and $S_{dz}(\omega_i)$ are the corresponding spectral displacements for frequency ω_i. The total response is found by implementing into SAP IV the Ten Percent method,[13] which is presented in Appendix B.

Because an acceleration field is desired for input to a more refined model, the psuedo acceleration given by $\{\ddot{U}_i\} = \omega^2 \{U_i\}$ is extracted and the total acceleration at a given node is found by the Ten Percent method. The resulting acceleration field is stored on a file for later use.

B. The Confinement Structure Model

The NFS confinement structure is a collection of massive interconnected reinforced concrete cells with wall and slab thicknesses that vary widely. It is unsymmetrical and possesses extremely massive walls and slabs; hence, it is not typical of the usual structure encountered in earthquake engineering analysis. The massive walls and slabs form cells that constitute a collection of short thick boxes interconnected to form the structure. Both the masses and the stiffnesses are very high.

The plant was modeled as a collection of floor and roof slabs composed of solid 8- to 21-variable-node isoparametric elements supported and connected by walls formed from quadrilateral and triangular plate elements. The entire structure can be modeled by the use of plate elements only; however, the three-dimensional slab elements were used to simplify the wall and slab nodal connections.

After the selection of the basic finite element model, a careful study was made of the construction drawings and details. All slabs that were to be included in the overall model along with their relative locations and significant dimensions were identified. A coordinate system was established, all significant nodal coordinates were located, the individual cells were modeled, and their connecting points were established. Large masses such as heavy shielding doors, heavy equipment, large liquid holding tanks and vessels, and significant piping were identified and represented as lumped masses at the proper nodal points.

The lack of symmetry and uniformity in the structure prevented the use of any automatic node and element data generation. Once the basic nodal coordinates and element data set were determined, several small preprocessing codes were used to insert additional nodal points or groups of nodal points from additional elements and to plot nodal point locations. Through the use of such routines and by careful checking and rechecking, the final plant model data were obtained. Boundary nodes and ground contact nodes were identified, and the program deleted the equilibrium equations associated with these nodes. The resulting model consisted of 474 nodal points, 74 solid elements, 157 plate elements, 26 rod or truss elements, and 120 lumped masses. Assembly of the equations at the element level and deletion of boundary node equations resulted in a system of 1191 equations with a maximum half bandwidth of 414.

The nonmonolithic connections were also considered in the modeling. A number of cells are not connected to each other in the usual structural sense but have a joint composed of a slab recessed into a wall and resting on the recess ledge. The slab and wall are separated by a layer of Rodofoam, which was assumed to be highly compressible. This type of connection has vertical stiffness but essentially no horizontal stiffnesses (neglecting friction) until enough relative motion occurs for the slab to contact the wall. This connection can be correctly modeled in the horizontal directions by the use of a bilinear spring, which requires a nonlinear structural code. Such codes are available, but they cannot accommodate large systems of equations. Also, a more costly time history method would be required for the solution. In this study, the motions were assumed to remain small enough that nonlinear effects would not invalidate the result. Thus, all nonmonolithic connections were modeled by the use of truss elements that have defined axial stiffnesses. The maximum relative motions at these connections will be discussed in a later section of this report.

C. Analysis Procedures

SAP IV was used to obtain the undamped natural frequencies of the structure and their corresponding mode shapes. The equations of motion were transformed to uncoupled modal equations. All modes with frequencies lower than 33 Hz were used in the analysis, and the response spectrum technique was used to solve the modal equations. The maximum modal displacement responses were calculated from the input response spectra shown in Figs. 19 and 20. The pseudo-modal accelerations were obtained from the modal displacements. The total responses were found by implementing into SAP IV the Ten Percent method.[13] The resulting spatial response components were then combined by the square-root-of-the-sum-of-the-squares method (SRSS).[13] Responses were obtained for earthquake intensities of 0.12 and 0.18 g's.

D. Results and Conclusions

The wooden facility model was used to identify the pertinent confinement structures in the early stages of this project. Figure 22 shows the visible edges of some elements used to model the plant. This information was derived from a code that was written to plot vectors between any set of given nodes. By exaggerating the modal displacements and calculating new coordinates of the displaced nodes, an indication of the mode shapes can also be obtained. The calculated natural frequencies for the first 24 modes are listed in Table IV and Figs. 23 through 46 show the corresponding mode shapes. The lowest natural frequency was 12.16 Hz.

An examination of the structure geometry reveals that certain mode shapes could have been

expected. The bending mode associated with a tall structure like the XPC, and the cantilever modes associated with the column-supported and cantilevered crane room attached to the PMC are examples. Other expected mode shapes require some imagination on the part of the analyst. The gap formed by the chemical crane room overhanging the SRC gives rise to a yawning mode that is shown in Fig. 32, mode 10.

The importance of the nonmonolithic connections is illustrated by examining the first mode shape that occurs at a frequency of 12.16 Hz (Fig. 23). This mode involves movement of the AC, LWC, and VWR in a swinging fashion. It results from the nonmonolithic connections between these cells and the XPC. Computer runs were also made in which all cells were connected monolithically and the bending mode associated with the XPC (Fig. 30) was the lowest mode. This was not considered to be as realistic as nonmonolithically modeled connections.

Table V shows the sum of the SRSS of the coordinate displacements at adjacent nodes that constitute a nonmonolithic connection. The nodal displacements are relative to the fixed base. The largest of these movements, the motion between the LWC and the wall of the XPC, was 1.1 mm (0.045 in.). Because all of these connections are separated by a 1.0-in. layer of Rodofoam, the motions are not considered large enough to cause any significant stiffness change. Therefore, the linear analysis performed is believed to be adequate. The effect of additional connection movements caused by local rocking of the cells will be addressed in a later section. Under the soil conditions that exist at this site, the relative motions of the facility confinement substructures are quite small compared to the pile cap motions. Therefore, a rigid body representation of the facility motion can be used to examine the stresses in the foundation piles.

The acceleration field from this model was used to examine concrete behavior in a more refined cell analysis presented in later sections.

IV. SUBSTRUCTURAL ANALYSIS

A. Introduction

SRSS displacements and accelerations adjusted for close frequencies were obtained at the nodes of the NFS confinement structural model. The finite element grid of this model was too coarse to consider the use of stresses. In addition, the stress resultants for the plate elements were not in a format convenient for use. The stress resultants were computed at the element centers, and rarely did their directions coincide with the directions of the global coordinates. Displacements can be obtained quite accurately through the use of a rather coarse finite element grid. Therefore, displacements were determined and the accelerations were obtained from these displacements through the use of natural frequencies.

Though usually the displacement field is used for obtaining stresses or stress resultants, several factors led us to use the acceleration field for this investigation. Ultimate loads, not stresses or displacements, are the primary quantities used in the mathematical treatment of reinforced concrete structural elements. The ultimate loads are normally based on average or mean stress distributions; hence, localized stress variations are disregarded. In addition, load-displacement relationships for reinforced concrete are difficult to establish and can yield unreliable results.

The use of SRSS acceleration fields and the structure's weight distribution to obtain inertial forces permits the inclusion of the effects of concentrated weights, such as equipment, without difficulty. Once the inertial load distribution has been determined, stress resultants at any point in a substructure can be determined from equilibrium considerations, provided the substructure is statically determinate. The analysis of statically indeterminate substructures becomes more complicated.

The SRSS accelerations and displacements at the nodal points of the confinement structure model were surveyed. The points displaying the

largest accelerations were noted as to cell and location within the cell. Cells were examined in sequence from the largest accelerations to the smallest. From the nodal SRSS accelerations, acceleration fields were obtained by averaging and by linear interpolation between nodal points. From the drawings of the cell and the equipment list, weight distributions along the three global axes were determined. The seismic forces acting on the cell were obtained as the product of the accelerations and the weights. Examples are shown in Figs. 47 through 52.

Once the seismic loads were determined, shears, moments, and axial forces were computed. The computed inertial stress resultants were then compared to the computed ultimate capacity of the section under consideration. The ultimate capacities of the reinforced concrete sections were calculated as described earlier. The initiation of failure was defined to occur when a seismically produced stress resultant in a structural element equaled its corresponding computed ultimate capacity.

B. Substructure or Structural Element Analyses

1. PMC. The cell subjected to the largest accelerations was the PMC, and in particular, the MCR, which constitutes the cantilevered north end of the PMC. The MCR is supported by two 0.6-m (2-ft)-diam concrete columns at the extreme north end. The relative lateral displacements of the columns for a 0.18 g's earthquake were small (1.2 mm or 0.047 in.), therefore the columns were not effective in resisting lateral seismic loads. The shear and moment at the critical section of the MCR were determined along with its estimated ultimate capacity. The location of the critical section is indicated in Fig. 49, and the computed shears and moments are given in Table VI.

The moment produced by the 0.18 g's seismic loads is larger than the ultimate moment. The cell section was not designed to resist a moment because the amount of steel reinforcing placed in the walls was small. A flexural section with a small percentage of steel reinforcing will possess a larger maximum uncracked moment than its computed ultimate moment. This was the case for the critical section of the MCR. The concrete tensile strength was determined by the formula given in the ACI Code.[1] The significance of the maximum elastic moment being larger than the ultimate moment is that if failure occurs, it will be sudden and complete.

By comparing the capacity of the MCR critical section with the seismic loads, an earthquake magnitude at which the onset of failure occurs was determined. A value of 0.14 g's was estimated as indicated in Fig. 53.

The total collapse of the MCR would not necessarily lead to a radioactive release. This section is separated from the rest of the PMC by a heavy shielding door. The door provides an equipment entry to the PMC and would normally not be open during operation of the PMC.

2. PMC and GPC Intersection. NFS consultants indicated that the intersection of the PMC and the GPC could be a critically loaded area with respect to shear forces. Lateral earth pressure shear loads resulting from the embedded GPC would be transmitted to the above-grade structure through this section. Figure 54 is a diagram of the intersection. The shear capacity of the intersection was based on the shear-friction concept. Comparison of seismic loads and the ultimate resisting loads indicates that the intersection is not critically loaded. The maximum calculated seismic and resisting shear forces acting at the intersections are given in Table VII.

3. Pile Analysis. The investigation of the vertical seismic loads on the piles was based on information obtained from the soil-structure study and from the seismic loads developed from the SRSS acceleration fields. The pile axial forces were determined directly from the element stress output from LUSH. The quadrilateral element used in LUSH yields acceptably accurate axial stresses, whereas the use of displacements introduces uncertainties with respect to the maximum stress. Displacement-time histories must be scanned to locate the largest displacement difference between adjacent nodal points. The maximum axial pile stresses are given in Table VIII. Considering the piles on the south side of the N-S model and the 0.18 g's earthquake, the seismic pile axial stress of 40.7 MPa (5900 psi)

is 65.6% of the dead load stress of 62.0 MPa (9000 psi). This value represents the stress from global rocking only.

The highest unit of the confinement structure contains the XPC (Fig. 3). It is also one of the narrowest units in the N-S direction. These conditions would tend to produce the largest pile stresses from local rocking. The overturning moment of the unit was determined from the inertial forces. This unit is connected to the AOC, the LWC, and the UPC. It is therefore statically indeterminate, and to obtain the overturning moment exactly requires consideration of deformations. In addition, this cell has several concrete block walls and steel frame members attached to it. The weights of these attached structural elements were included in the confinement structure analysis and the soil-structure system, but their stiffnesses were neglected. The stiffnesses contributed by these structural elements would act to prevent overturning of the XPC. Consideration of all restraints would require a complicated analysis; however, an upper bound was simple to obtain by assuming that the piles resisted the entire overturning moment. A partial compensation for restraints was realized by assuming that the piles were located at the extreme edges of the cells. Through the use of the total computed overturning moment, the pile stresses were calculated for local rocking. The seismic pile stresses were calculated to be 52% of the dead load stresses for an 0.18 g's earthquake. Therefore, this conservative estimate indicates that the combined effect of local and global rocking from a 0.18 g's earthquake produces stresses that are approximately 1.18 times the dead load axial pile stresses. The pile caps were not designed to transmit tension to the piles; hence, the cell would tend to lift off the piles. For the 0.12 g's earthquake, the seismic-induced axial load was estimated to be 69% of the dead load. The earthquake level that would result in zero axial stresses in the piles on one side of the XPC was 0.16 g's (Fig. 55).

Rigid body displacements of the XPC caused by rocking about its E-W axis were estimated for an earthquake level of 0.14 g's. At this level, 83% of the XPC weight is acting on the piles along one side and 17% on the piles along the other side. Through the use of these values, the maximum XPC rocking displacement at an elevation of 14.6 m (48 ft) (the top of the CPC) was estimated to be 18.3 mm (0.72 in.). The calculations are given in Appendix A-IV. The 25.4-mm (1.0-in.) Rodofoam-filled gap between the XPC and CPC is situated 45° to both cells; hence, the maximum distance either structure must move to close the gap is 36 mm (1.42 in.) A comparison of the relative acceleration responses and geometries of the two cells shows that the maximum rocking displacement of the CPC would be much less than the XPC displacement. Considering the Rodofoam-filled gap and the estimated cell displacements, pounding of the two cells can be disregarded as a major concern. The load-displacement characteristics of the Rodofoam are unknown; however, it is probably a highly compressible material. If the Rodofoam can be compressed to one-half its thickness without introducing large nonlinearities, the linear modeling of the nonmonolithic connections will not introduce serious inaccuracies.

The lateral loads acting on the piles were also investigated. The first attempt at obtaining the lateral loads was based on the displacements generated by LUSH. A computer program was written that used the displacement field as input and yielded the pile moment distribution, the lateral soil pressure distribution, and the lateral pile cap load. The lateral pile cap loads obtained from the computer program were smaller than the average lateral loads obtained using the site maximum acceleration. In obtaining the average pile cap lateral load, the facility was assumed to act as a rigid body. The relatively large distances between deflection data points coupled with the large lateral force and moment gradients near the pile tops would yield inaccurately computed lateral pile cap loads. In addition, the computed lateral soil pressures near the pile tops greatly exceeded the pressure that the soil could realistically resist. This approach did indicate that an elastic solution of the pile-soil system was not valid for the magnitude of the seismic loads considered.

Because yielding of the soil near grade would occur, a pile lateral load capacity method that considered plastic action was required. The displacements are assumed to be sufficiently large for passive earth pressure to develop. The upper soil layer was described as a mixture of gravel, sand, and silt, all of which are generally cohesionless soils. Brom's method[14] was used to compute the pile lateral loads in the cohesionless soils. The angle of internal friction for the soil layer was computed as 40° from the information obtained from site investigations.[10] The only soil parameters required were the angle of internal friction and the soil density. The computed ultimate pile lateral loads for the strong and weak axes of the pile section are given in Table IX.

The lateral loads on the piles were obtained from LUSH results and the site horizontal accelerations. The maximum lateral soil pressure force on the buried cell (the GPC) was used to obtain an equivalent passive earth pressure coefficient. The results from the N-S soil-structure system model were used because this two-dimensional model was a better representation of the confinement structure than the E-W model. The lateral forces on the buried cell were calculated indirectly from the shear forces in the GPC model elements at grade level. The average pile lateral force was obtained by subtracting the loads caused by earth pressure from the total lateral seismic load for the entire facility and then dividing by the total number of piles less the number of piles under the GPC. The effect of these piles was already included in determining the lateral forces on the GPC. The average pile lateral loads caused by seismic motions are also given in Table IX.

Once the vertical and lateral pile loads caused by the three earthquake components were determined, a procedure for combining them was needed. The question of failure criteria arose. The piles were subjected to biaxial bending in combination with an axial load; however, an interaction diagram would not be very useful. The maximum moments and the axial compressive force do not occur simultaneously nor at the same location along the pile axis. Determining the moments and axial force for a given point would be difficult, if not impossible. Bending moments from the seismic loads would be required to obtain stresses. The difficulty in this approach is that the soil pressure on the piles would be different than that assumed for the ultimate lateral loads. In the absence of established failure criteria for dynamically loaded piles, the ratios of seismic loads to ultimate loads were computed and the most severe combination of SRSS values was obtained. These ratios for the different cases are given in Table X. In one case, the average seismic pile lateral load exceeded the lateral ultimate capacity of the piles in the weak axis. The load in excess of the ultimate weak axis lateral load was redistributed to the strong axis piles before the load ratios were computed. The load ratio could not exceed unity. The most severe SRSS combinations of the load ratios are also given in Table X. A value of unity indicates the piles at maximum capacity, and this corresponds to an earthquake magnitude of 0.14 g's as indicated in Fig. 56.

Yielding of a part of the piles in flexure would not necessarily lead to failure of the facility. The facility has not failed if the confinement integrity has been maintained. The piles are confined by the soil mass and the structure; hence, they cannot collapse. Yielding could have a beneficial effect in that the energy dissipation could reduce the seismic response of the facility. Collapse of the piles would depend upon the number of stress reversals they would undergo.

V. METHODS AND ASSUMPTIONS

The goal of this investigation was a realistic assessment of the confinement structure seismic capability. The accuracy of this assessment is strongly dependent upon the methods of analysis, the modeling of the structure, and the characteristics of the site earthquake motions. Consequently, the known, probable, or unknown effects on the structural response resulting from the use of specific methods, procedures, or input are discussed.

1. The NRC Design Response Spectra as given in Regulatory Guide 1.60 were used as the basis

for the seismic input. The response spectra of generated acceleration time histories were developed to envelope the NRC Design Response Spectra. Recent studies indicate that the use of the seismic criteria in Regulatory Guide 1.60 is overly severe in the seismic evaluation of a site.[15,16] In addition, the dominant frequencies predicted by calculation are generally higher than those actually recorded. Both the larger site response and the higher frequency would lead to a higher foundation level response spectrum for the site under consideration. Additional response severity resulted from the enveloping of the nodal response spectra to obtain the foundation level response spectrum and the SRSS combination of the spatial components. The combination of the vertical response and the greatest horizontal response seems more realistic. The SRSS method as applied does not consider the directional characteristic of earthquakes.

2. The confinement structure was modeled with three-dimensional solid and plate elements. The rotational degrees of freedom at connecting nodes between plate and solid elements were deleted. Consequently, the edges of the plate elements connecting to either floors and roofs could not rotate. The finite element model would therefore predict lateral stiffnesses and natural frequencies greater than those possessed by the actual structure. Increased natural frequencies would tend to decrease the structural response. For the NFS confinement structure, the roofs and floors are relatively narrow, and their depth to shortest span ratios are relatively large. Hence, the effect of deleting the rotational degrees of freedom would be minor.

3. A linear analysis of the facility was used. The relative displacements within the facility were small, and according to calculations, the first component to fail was uncracked up to failure. Therefore, the linear solution is essentially valid to the point of failure. Use of a linear analysis for evaluating a facility with nonlinearities could lead to either over- or underestimating the seismic responses. Energy dissipation would result in a lower response, but the decrease in natural frequencies would tend to increase the response. Probably the energy dissipation effect (damping) would dominate, so the linear analysis would result in larger responses.

4. Three-dimensional soil-structure effects were not realized in the analysis procedure used. The confinement cells are interconnected so that torsion (twisting about the vertical axis) may produce a significant response. No estimate of this effect is available. Three-dimensional effects caused by unidirectional motions were included in the analysis of the confinement structure.

5. The confinement structure was considered to be a fixed-base structure in the dynamic analysis. Structural responses caused by rocking motions are neglected in this analysis. Several studies have been made to determine the effect of this assumption on structural responses.[15,16] They have indicated that the structural responses from rocking motions are generally less severe than those obtained by assuming a fixed base in the absence of torsional effects. Using the results reported in Ref. 15, slightly lower response magnitudes could have been expected had the analysis incorporated a flexible foundation.

6. The water table was assumed to be 22.9 m (75 ft) below grade; however, the water table may be near the ground surface. Another possibility is that a perched water table exists at the site. Assuming that the water table was near the ground surface would have resulted in a softening of the site. The cohensionless upper and lower soil layers would have smaller grain-to-grain pressures. This would tend to reduce the dominate frequency of the soil. For this facility, a decrease in soil dominant frequency would have reduced the foundation level response and led to less severe conditions.

7. During construction 12.7-mm (1/2-in.)-thick insulating fiberboard was installed around the GPC walls. This insulating fiberboard was assumed to remain intact; however, it may have deteriorated. If it deteriorated, the lateral pile forces would tend to be larger, particularly in the N-S direction. The absence of the fiberboard would

not lead to large increases in lateral pile loads because it is relatively thin.

8. In analyzing the piles, we assumed that they would be isolated. The spacing of the piles in certain regions was such that this assumption may not be valid. Pile groups possess a smaller lateral load capacity than the same number of piles located individually. Also, the capacity of the piles is dependent on the number of lateral force directional changes. The lateral load capacity decreases with the number of load reversals.

9. There is uncertainty about the failure mode and criteria associated with embedded piles. The procedure used for evaluating failure may not be correct.

Considering the assumptions and methods used in the plant confinement structure seismic evaluation and their potential influence on the seismic responses, the value of 0.14 g's for failure of the first structural element is believed to represent a lower bound. Another failure mode not considered in this analysis is that of a vertical settlement causing differential displacements leading to cracking in the cell walls. This failure mode would be difficult to evaluate.

VI. SUMMARY OF RESULTS

A dynamic analysis of the NFS Fuel Reprocessing Plant was conducted. The free-field input was taken as the NRC Design Response Spectra. LUSH was used to obtain foundation level seismic response spectra to excite a fixed-base finite element model of the facility. SAP IV was used to obtain the structural response of the confinement structure. The modal response was obtained by the SRSS method with adjustments for close frequencies. The structural analysis was linear; hence, only the onset of failure could be determined.

Listed below is a cell-by-cell summary of the results obtained in this study. The lateral pile failure onset predicted from the investigation was based on the assumption of rigid body foundation displacements. Therefore, the g-level reported for lateral pile failure is the same for all cells directly supported by piles.

The maximum g-level used in the analysis was 0.18 g's. Structural element loading conditions are given for earthquake levels up to 0.20 g's in this section. Extrapolation was used to obtain conclusions regarding cell status at 0.20 g's.

A. Acid and Off-Gas Recovery Cell (AOC)

Parts of this cell are enclosed by concrete block walls whose shear strength is relatively low in comparison to that of reinforced concrete walls. The portion of this cell that is enclosed by concrete block walls was not considered a confinement structure; hence, it was not included in the seismic analysis. The part enclosed by reinforced concrete walls was considered a confinement structure and was included in the analysis. Lateral pile failure was predicted to occur at 0.14 g's. No other failure type was predicted for earthquake levels below 0.20 g's.

B. Chemical Process Cell (CPC)

Lateral pile failure was predicted to occur at 0.14 g's. No other type of failure was predicted for earthquake levels below 0.20 g's.

C. Analytical Cells (AC)

No part of this cell structure was found to fail for earthquake levels below 0.20 g's.

D. Equipment Decontamination Room (EDR)

Lateral pile failure at 0.14 g's was the only failure type predicted for earthquake levels below 0.20 g's.

E. Extraction and Product Purification Cells (XPC)

Lateral pile failure was found to occur at 0.14 g's. Pile tension failure was found to occur at a lower bound value of 0.16 g's; however, overturning of this cell was not considered credible for earthquake levels below 0.20 g's. A nonmonolithic connection exists between the XPC and the CPC. Serious pounding of this joint is not anticipated below 0.20 g's; however, piping connecting the XPC with the other cells could be damaged at lower earthquake levels.

F. General Purpose Cell (GPC)

Lateral pile failure was predicted at 0.14 g's. No other failure type is anticipated for earthquake levels below 0.20 g's.

G. Liquid Waste Cell (LWC)

Lateral pile failure at 0.14 g's is the only failure type predicted for earthquake levels below 0.20 g's.

H. Mechanical Crane Room (MCR)

This room is discussed in conjunction with the Process Mechanical Cell.

I. Process Mechanical Cell (PMC)

The MCR forms the north end of this cell. The MCR was designed for storage and maintenance of the traveling crane that services the PMC. It is separated from the rest of the PMC by a heavy shielding door that is normally closed during cell operation. The MCR could completely separate from the PMC at a section north of the shielding door at 0.14 g's; however, confinement integrity of the "hot" part of the PMC would be maintained, provided that the shielding door was closed. Lateral pile failure was predicted to occur at 0.14 g's. No other failures were predicted for earthquake levels below 0.20 g's.

J. Scrap Recovery Cell (SRC)

This cell is monolithically attached to the CPC and is therefore considered a part of the CPC.

K. Uranium Product Cell (UPC)

Lateral pile failure was predicted to occur at an earthquake level of 0.14 g's. No other failures were predicted below 0.20 g's.

L. Ventilation Wash Room (VWR)

No failures of any type were predicted for this room for earthquake levels below 0.20 g's.

VII. FUTURE INVESTIGATIONS

The need for additional information became evident in the evaluation of the piles. Knowledge of pile behavior and modeling procedures for piles subjected to seismic motions is lacking. The information presently available is not applicable in that the lateral cap load is assumed to be the applied load and the resulting soil pressure is assumed to be the reaction load. Here, the soil pressure is the applied load and the lateral cap load is the reaction. A failure criterion does not exist for piles subjected to combined axial loads and biaxial bending.

We were unable to find guidance for modeling the three-dimensional reprocessing facility into two-dimensional soil-structure systems. In the future this may not be important, because reprocessing plants designed to meet seismic requirements should be more symmetrical and adaptable to two-dimensional modeling. A properly modeled facility is one of the most important aspects of an analysis, and without it, the results are difficult to assess.

The effects of a perched water table are unknown, and no published studies were located in the literature search on this topic. The use of piles under the facility would appear to de-emphasize the importance of a perched water table.

REFERENCES

1. "Building Code Requirements for Reinforced Concrete," ACI 318-71, American Concrete Institute, Detroit, Michigan (1971).
2. J. Lysmer, Takekazu Udaka, H. Bolton Seed, and Richard Hwang, "LUSH - A Computer Program for Coupled Response Analysis of Soil-Structure Systems," University of California report EERC 74-4 (April 1974).
3. Design Response Spectra for Nuclear Power Plants, USAEC Regulatory Guide 1.60 (1973).
4. M. Watabe, "SIMEAR - Generation of Simulated Earthquakes," National Information Service Document No. 09-573 (1972).
5. P. B. Schnabel, J. Lysmer, and H. B. Seed, "SHAKE - A Computer Program for Earthquake Response Analysis of Horizontally Layered Sites," University of California report EERC 72-12 (December 1972).
6. Damping Values for Seismic Design of Nuclear Power Plants, USAEC Regulatory Guide 1.61 (1973).
7. R. H. Scanlon and K. Sachs, "Earthquake Time Histories and Response Spectra," J. Eng. Mech. Div., Amer. Soc. Civ. Eng. 100 (EM4), 635-655 (August 1974).
8. Houshang Dezfulian and H. Bolton Seed, "Seismic Response of Soil Deposits Underlain by Sloping Rock Boundaries," J. Soil Mech. Found. Div., Amer. Soc. Civ. Eng. 96 (SM6), 1893-1916 (November 1970).

9. Victor Liang, "Dynamic Response of Structures in Layered Soils," National Technical Information Service report PB-236 449 (January 1974).

10. Application for Amendments to Provisional Operating License No. CSF-1 for the NFS West Valley Reprocessing Facility, Supplement No. 4, Nuclear Fuel Services, Inc., Rockville, Maryland (1974), Docket No. 50-201.

11. Application for Amendments to Provisional Operating License No. CSF-1 for the NFS West Valley Reprocessing Facility, Volume 1, Nuclear Fuel Services, Inc., Rockville, Maryland (1974), Docket No. 50-201.

12. K. Bathe, E. L. Wilson, and F. E. Peterson, "SAP-IV - A Structural Analysis Program for Static and Dynamic Response of Linear Structures," University of California report EERC 73-11 (1973).

13. Combining Modal Responses and Spatial Components in Seismic Response Analysis, USNRC Regulatory Guide 1.92 (1976).

14. Bengt B. Broms, "Lateral Resistance of Piles in Cohensionless Soils," J. Soil Mech. Found. Div., Amer. Soc. Civ. Eng. 90 (SM3), 123-156 (May 1964).

15. M. A. Sarrazin, J. M. Roesset, and R. V. Whitman, "Dynamic Soil-Structure Interaction," J. Struct. Div., Amer. Soc. Civ. Eng. 98 (ST7), 1524-1544 (July 1972).

16. R. A. Parmelee, D. S. Perelman, S. L. Lee, and L. M. Keer, "Seismic Response of Structure-Foundation Systems," J. Eng. Mech. Div., Amer. Soc. Civ. Eng. 94 (EM6), 1295-1315 (December 1968).

BIBLIOGRAPHY

Izzat M. Idriss and Khosrow Sadigh, "Seismic SSI of Nuclear Power Plant Structures," J. Geot. Eng. Div., Amer. Soc. Civ. Eng 102 (GT7), 663-682 (July 1976).

Seismic Input, USNRC Standard Review Plan, Section 3.7-1, Office of Nuclear Reactor Regulation (June 1975).

H. B. Seed, J. Lysmer, and R. Huang, "Soil-Structure Interaction Analyses for Seismic Response," J. Geot. Eng. Div., Amer. Soc. Civ. Eng. 101 (GT5), 439-457 (May 1975).

H. Bolton Seed, I. M. Idriss, and Fred W. Kiefer, "Characteristics of Rock Motions during Earthquakes," J. Soil Mech. Found. Div., Amer. Soc. Civ. Eng. 95 (SM5), 1199-1218 (September 1969).

Dana Young, "Response of Structural Systems to Ground Shock," Colloquim Paper on Shock and Structural Response, Amer. Soc. Mech. Eng., New York, November 30, 1968.

J. S. Teraszkiewincz, "Seismic Dynamic Parameter Study on Finite Element Model of Nuclear Power Plant Facility," International Symposium on Earthquake Structural Engineering, St. Louis, Missouri, August 1976.

R. W. Clough, "Earthquake Analysis by Response Spectrum Superposition," Bull. Seis. Soc. Amer. 52, 647-660 (July 1972).

Seismic System Analysis, USNRC Standard Review Plan, Section 3.7-2, Office of Nuclear Reactor Regulation (June 1975).

TABLE I

SHEAR MODULI FOR LUMPED PILES

Model	Direction	Pile Shear Moduli, MPa (Kips/ft^2) Pile Number 1	2	3	4
N-S	Vertical	2010 (42 000)	4070 (85 000)	3160 (66 000)	1050 (22 000)
	Horizontal	445 (9300)	627 (13 100)	488 (10 200)	656 (13 700)
E-W	Vertical	1680 (35 000)	2780 (58 000)	2780 (58 000)	1240 (26 000)
	Horizontal	584 (12 200)	426 (8900)	426 (8900)	421 (8800)

TABLE II

POISSON'S RATIO AND DENSITY FOR EACH SOIL LAYER

Layer	Poisson's Ratio Static	Dynamic	Density Kg/m^3	(pcf)
GM/ML	0.30	0.45	2080	(130)
CL	0.35	0.45	2080	(130)
GM/ML	0.30	0.45	2160	(135)

TABLE III

MAXIMUM RESPONSES

Nodal Points (North-South Model)	Case I High Pile Stiffness: Maximum Acceleration Response (g's)	Frequency (Hz)	Case II Average Pile Stiffnesses: Maximum Acceleration Response (g's)	Frequency (Hz)
67	0.91	7.98	2.52	6.34
113	0.99	7.98	2.09	6.34
162	0.92	8.96	2.12	6.34
184	0.71	8.96	3.02	6.34

TABLE IV

NATURAL FREQUENCIES USED IN ANALYSIS OF FACILITY

Mode Number	Frequency (Hz)	Period (s)
1	12.16	0.0822
2	16.15	0.0619
3	16.59	0.0603
4	16.87	0.0593
5	18.05	0.0554
6	18.89	0.0529
7	19.78	0.0506
8	20.91	0.0478
9	21.85	0.0458
10	22.95	0.0436
11	24.18	0.0414
12	24.74	0.0404
13	24.87	0.0402
14	25.25	0.0396
15	26.56	0.0376
16	27.26	0.0367
17	27.68	0.0361
18	28.88	0.0346
19	29.39	0.0340
20	30.14	0.0332
21	30.17	0.0331
22	31.66	0.0316
23	31.92	0.0313
24	32.12	0.0311

TABLE V

DISPLACEMENTS AT NONMONOLITHIC CONNECTIONS

Nonmonolithic Connection No.	Connecting Nodes	Sum of SRSS Displacements in Nonmonolithic Directions: X (mm)	X (in.)	Y (mm)	Y (in.)
1	81-82	0.203	0.008	0.152	0.006
2	83-84	0.203	0.008	0.152	0.006
3	89-90	0.559	0.022	0.381	0.015
4	85-86	0.533	0.021	0.279	0.011
5	87-88	0.533	0.021	0.254	0.010
6	138-140	0.508	0.020	0.330	0.013
7	196-196	0.432	0.017	0.330	0.013
8	231-234	0.356	0.014	0.330	0.013
9	117-118	1.067	0.042	0.737	0.029
10	288-289	0.432	0.017	0.457	0.018
11	284-293	0.406	0.016	0.356	0.014
12	107-108	1.016	0.040	0.610	0.024
13	103-104	1.067	0.042	0.406	0.016
14	105-106	1.067	0.042	0.457	0.018
15	120-121	1.143	0.045	0.457	0.018
16	122-123	1.143	0.045	0.533	0.021
17	99-100	0.254	0.010	0.254	0.010
18	101-102	0.305	0.012	0.356	0.014
19	154-168	1.092	0.043	0.584	0.023
20	166-245	0.432	0.017	0.356	0.014
21	176-239	0.432	0.017	0.330	0.013
22	156-184	0.356	0.014	0.356	0.014
23	158-182	0.356	0.014	0.254	0.010

TABLE VI

SHEARS AND MOMENTS IN CRITICAL SECTION OF PCR

Stress Resultant	Earthquake Level 0.12g's	0.18g's	Ultimate
Shear, MN	2.98	4.45	3.48
(lbs)	(0.67×10^6)	(1.00×10^6)	($0.78\ 10^6$)
Moment, MN.m	14.14	21.57	10.28 (16.81)*
(lb-ft)	(10.43×10^6)	(15.91×10^6)	7.58×10^6 (12.4×10^6)*

*Denotes maximum elastic moment

TABLE VII

SHEAR AT INTERSECTION OF CFC AND PHC

Stress Resultant	Earthquake Level 0.12g's	0.18g's	Ultimate
Shear, MN	14.14	18.10	48.0
(lbs)	(3.18×10^6)	(4.07×10^6)	(10.8×10^6)

TABLE VIII

MAXIMUM AXIAL PILE STRESSES RESULTING FROM GLOBEL ROCKING

Model	Acceleration 0.12g's	0.18g's
N-S, MPa	25.64	40.68
(psi)	(3720)	(5900)
E-W, MPa	19.37	44.96
(psi)	(2810)	(6520)

TABLE IX

PILE LATERAL LOADS

Model	Acceleration 0.012g's	0.18g's	Ultimate Loads Strong Axis	Weak Axis
N-S, KN (lbs)	35.81 (8 050)	53.24 (11 970)	206.70 (46 470)	118.67 (26 480)
E-W, KN (lbs)	94.52 (21 250)	125.39 (28 190)	206.70 (46 470)	118.67 (26 680)

TABLE X

SEISMIC LOADS TO ULTIMATE LOAD RATIOS

Direction	Pile Axis	Accelerations 0.12g's	0.18g's
N-S	Weak	0.300	0.449
	Strong	0.173	0.258
E-W	Weak	0.797	1.000
	Strong	0.457	0.628
Vertical	-	0.42	0.55
Most Severe SRSS Combination		0.92	1.17

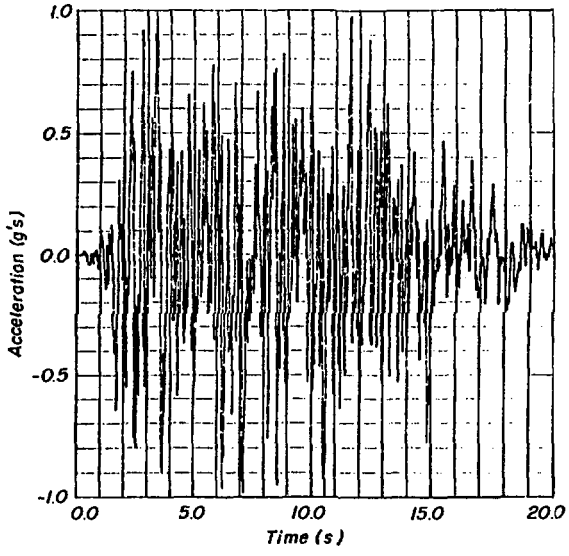

Fig. 1. Horizontal free-field ground motion accelerogram.

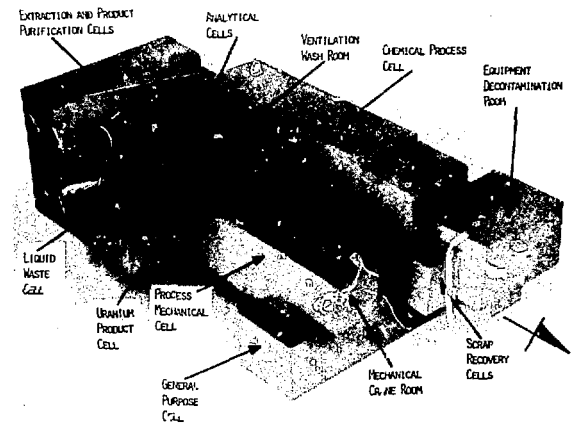

Fig. 3. View of confinement structure model.

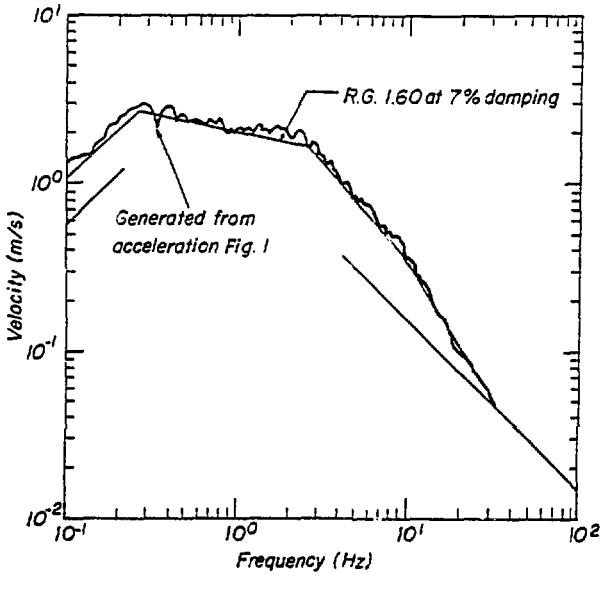

Fig. 2. Horizontal free-field ground motion response spectrum.

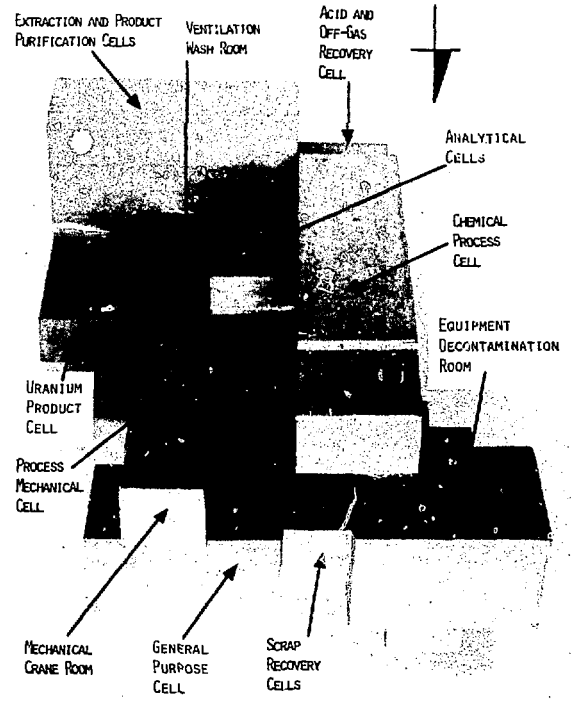

Fig. 4. End view of confinement structure model.

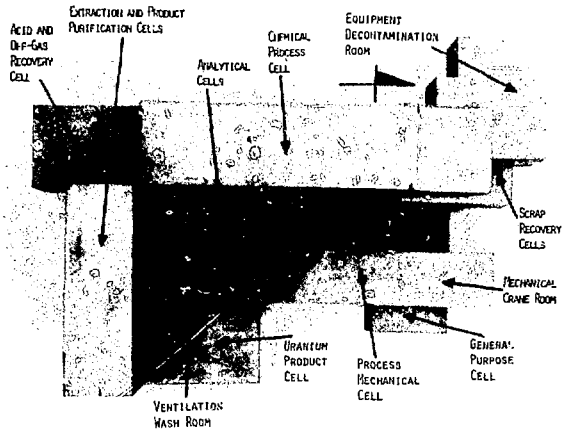

Fig. 5. Top view of confinement structure model.

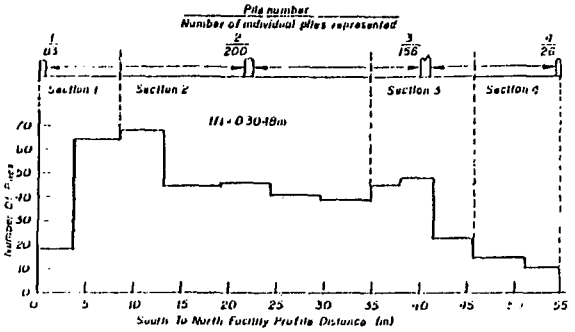

Fig. 8. Pile distribution and lumping in the N-S direction.

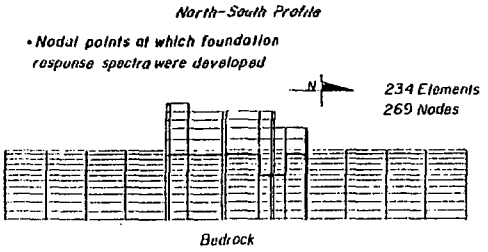

Fig. 6. N-S soil-structure finite element model.

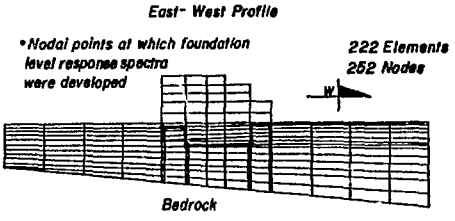

Fig. 7. E-W soil-structure finite element model.

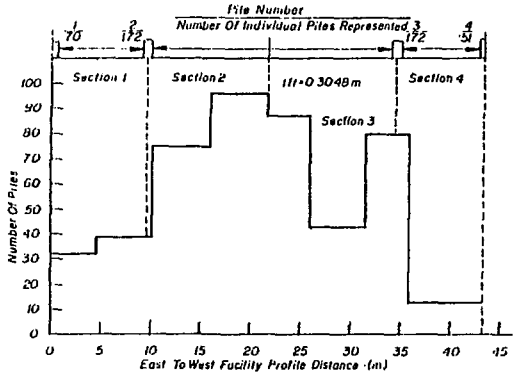

Fig. 9. Pile distribution and lumping in the E-W direction.

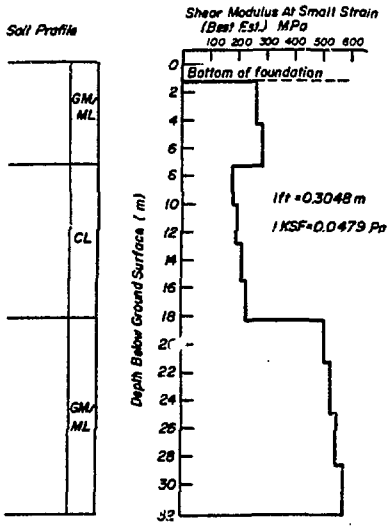

Fig. 10. Shear moduli at small strain vs depth for one-dimensional soil-structure interaction analysis.

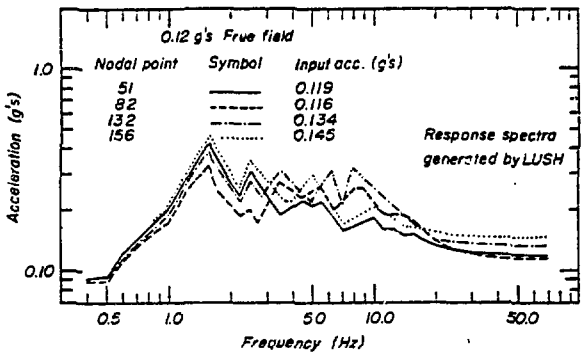

Fig. 12. Horizontal nodal response spectra for E-W model.

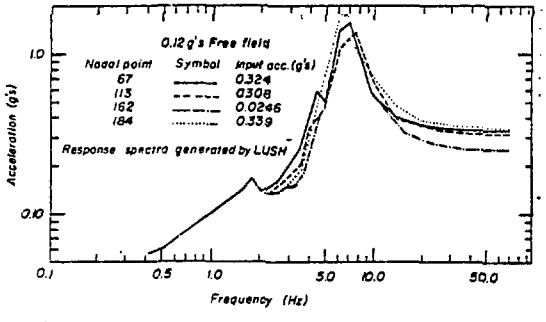

Fig. 13. Vertical nodal response spectra for N-S model.

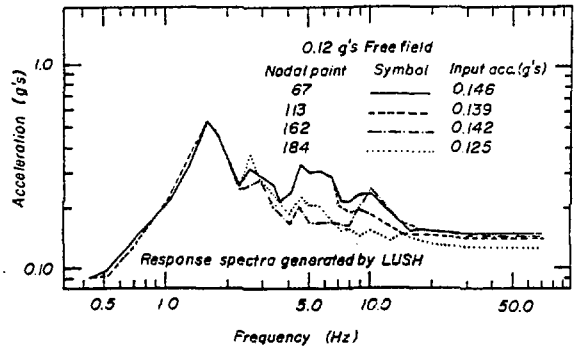

Fig. 11. Horizontal nodal response spectra for N-S model.

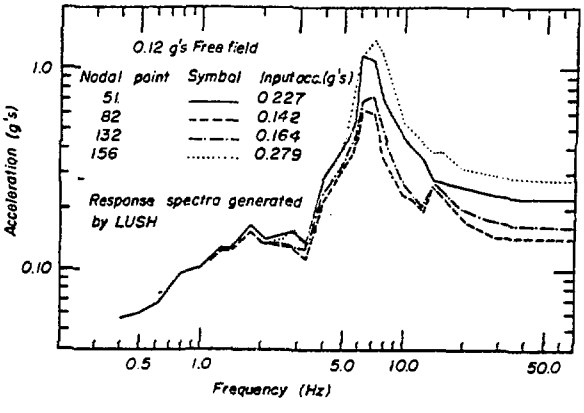

Fig. 14. Vertical nodal response spectra for E-W model.

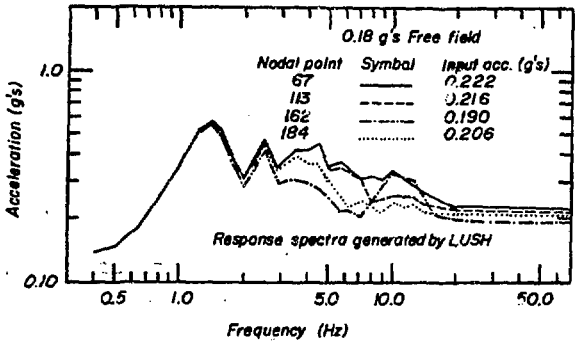

Fig. 15. Horizontal nodal response spectra for N-S model.

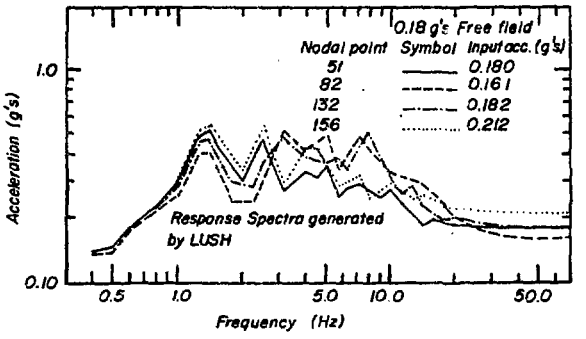

Fig. 16. Horizontal nodal response spectra for E-W model.

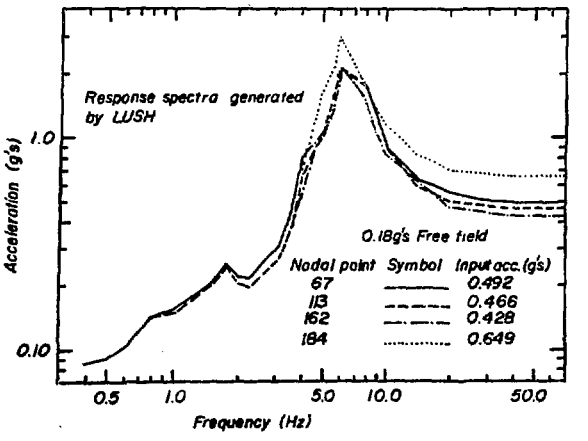

Fig. 17. Vertical nodal response spectra for N-S model.

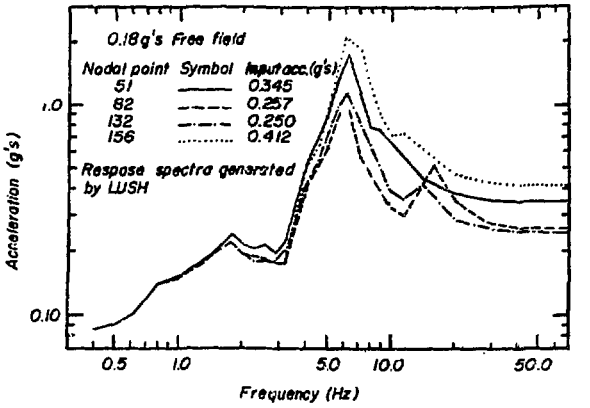

Fig. 18. Vertical nodal response spectra for E-W model.

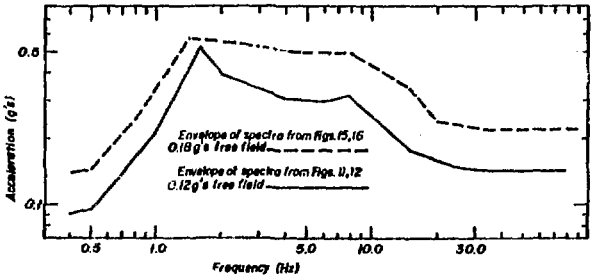

Fig. 19. Horizontal response spectra, 7% damping.

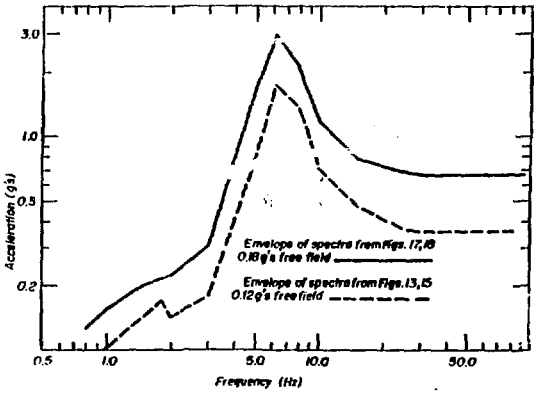

Fig. 20. Vertical response spectra, 7% damping.

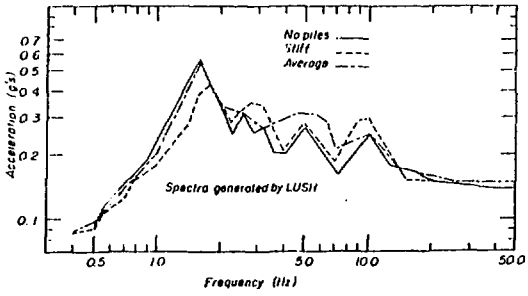

Fig. 21. Horizontal response spectra for different pile flexural stiffnesses.

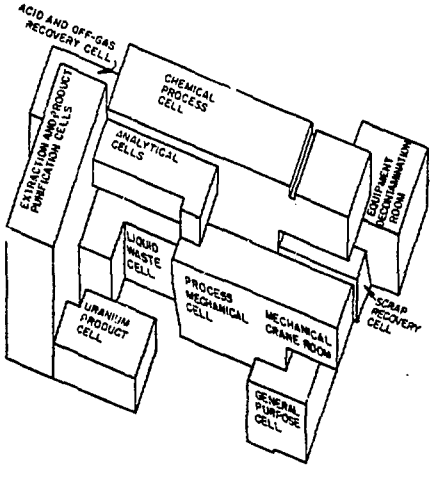

Fig. 22. Undistorted computer-generated view of confinement structure.

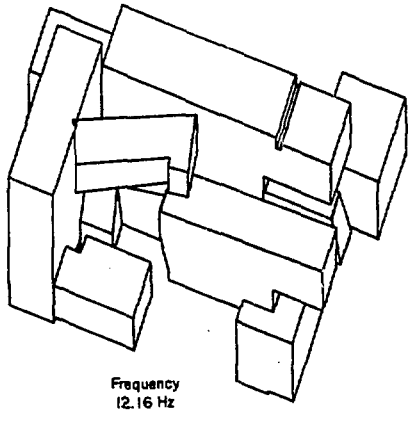

Fig. 23. First-mode shape.

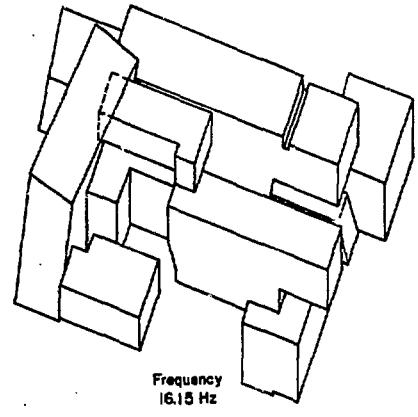

Fig. 24. Second-mode shape.

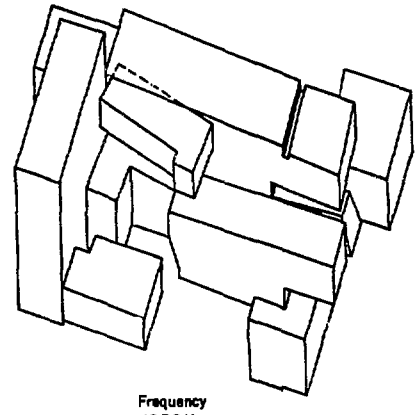

Fig. 25. Third-mode shape.

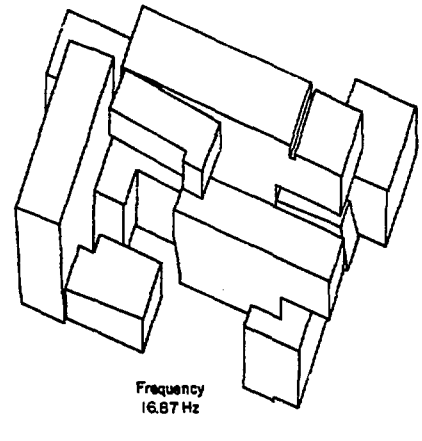

Fig. 26. Fourth-mode shape.

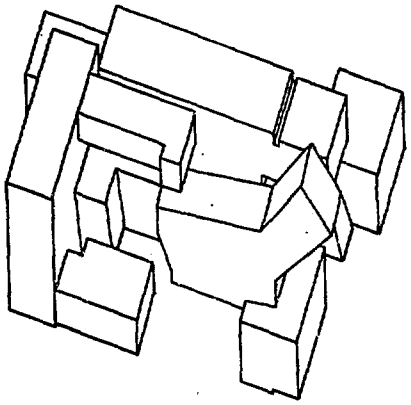

Frequency
18.05 Hz

Fig. 27. Fifth-mode shape.

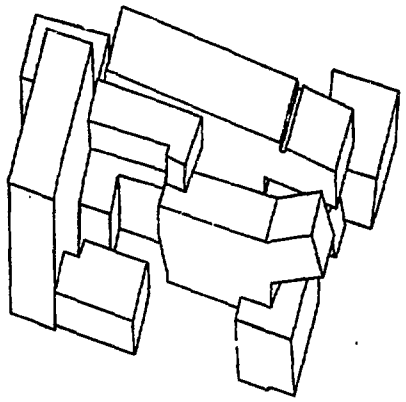

Frequency
19.78 Hz

Fig. 29. Seventh-mode shape.

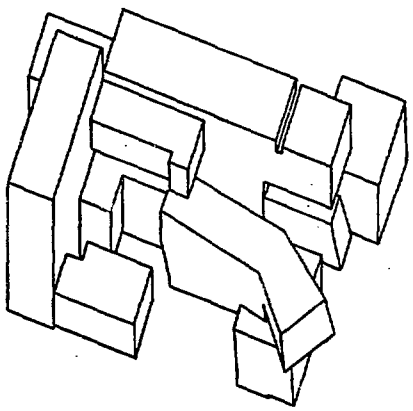

Frequency
18.89 Hz

Fig. 28. Sixth-mode shape.

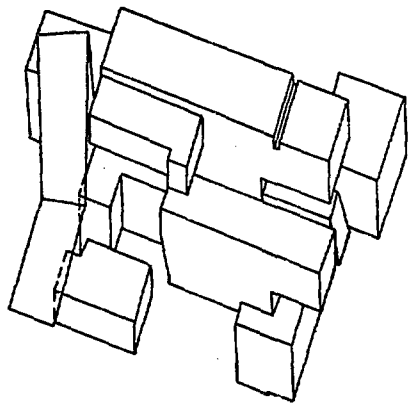

Frequency
20.91 Hz

Fig. 30. Eighth-mode shape.

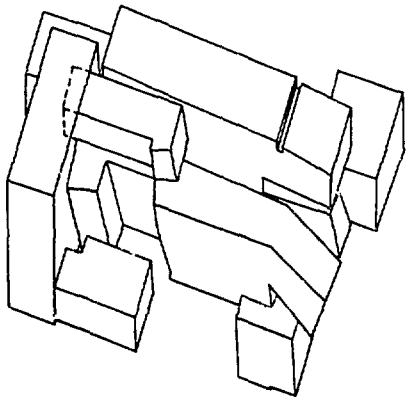

Fig. 31. Ninth-mode shape.

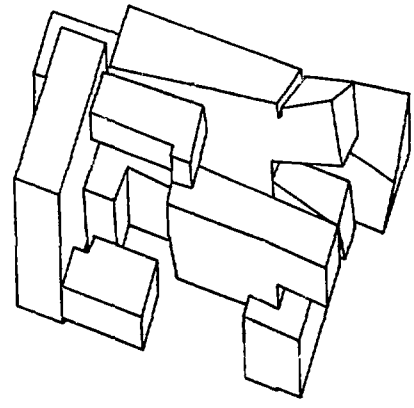

Fig. 32. Tenth-mode shape.

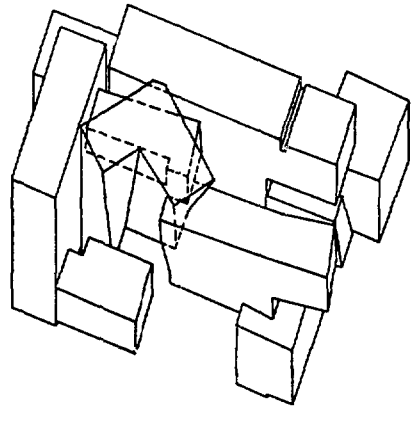

Fig. 33. Eleventh-mode shape.

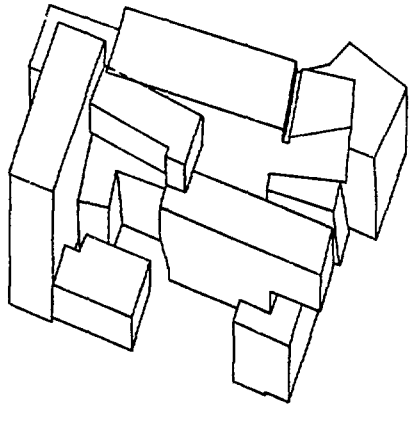

Fig. 34. Twelfth-mode shape.

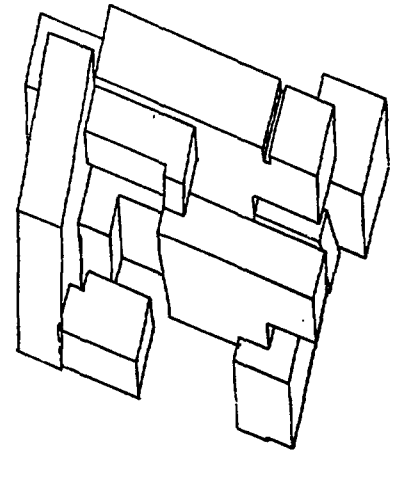

Fig. 35. Thirteenth-mode shape.

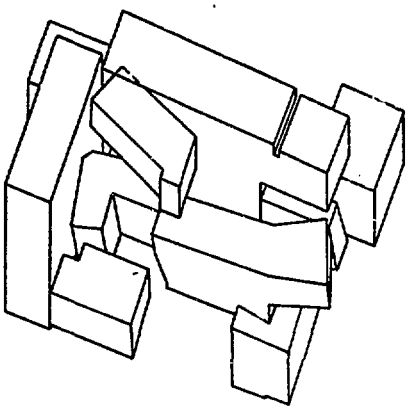

Frequency
25.25 Hz

Fig. 36. Fourteenth-mode shape.

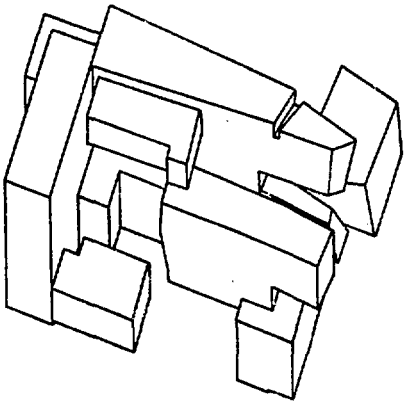

Frequency
26.56 Hz

Fig. 37. Fifteenth-mode shape.

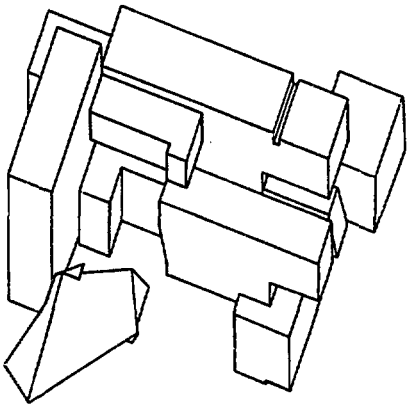

Frequency
27.26 Hz

Fig. 38. Sixteenth-mode shape.

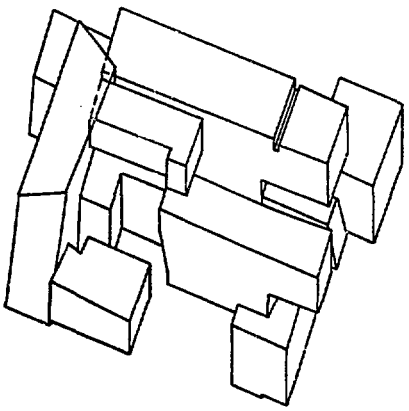

Frequency
27.68 Hz

Fig. 39. Seventeenth-mode shape.

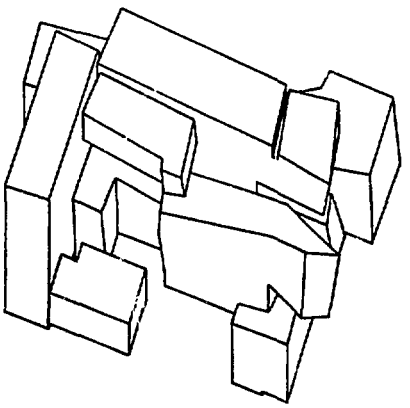

Frequency
28.98 Hz

Fig. 40. Eighteenth-mode shape.

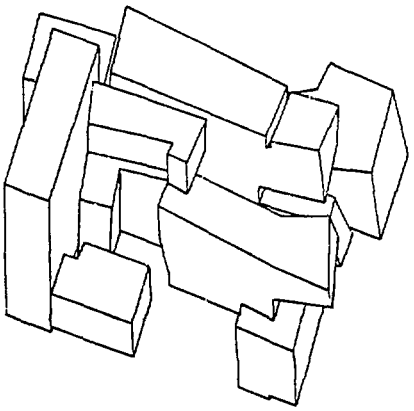

Fig. 41. Nineteenth-mode shape.

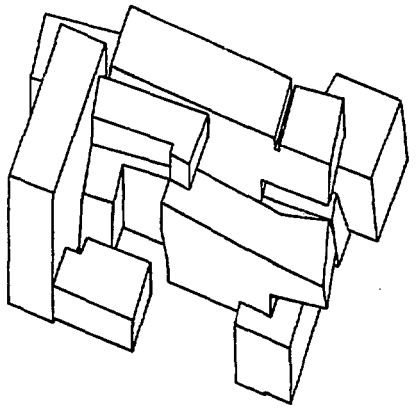

Fig. 42. Twentieth-mode shape.

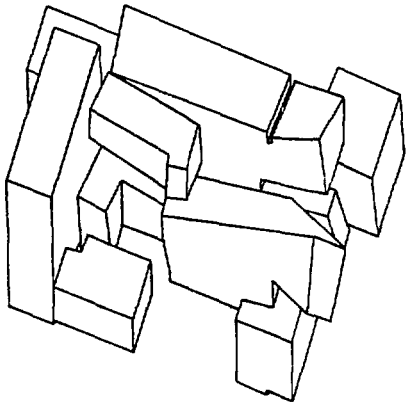

Fig. 43. Twenty-first-mode shape.

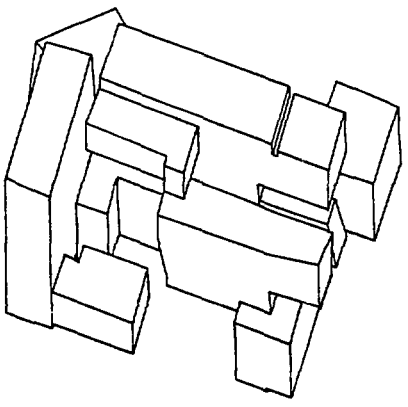

Fig. 44. Twenty-second-mode shape.

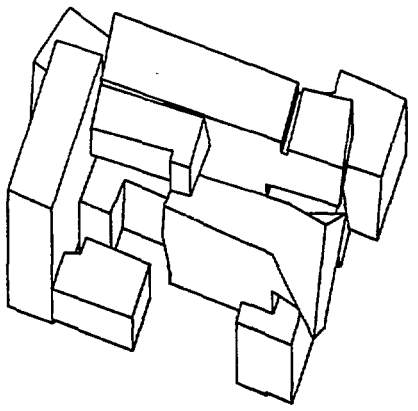

Fig. 45. Twenty-third-mode shape.

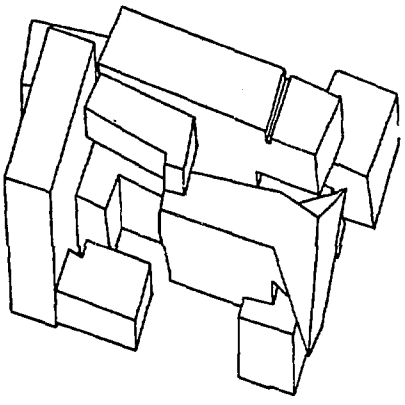

Fig. 46. Twenty-fourth-mode shape.

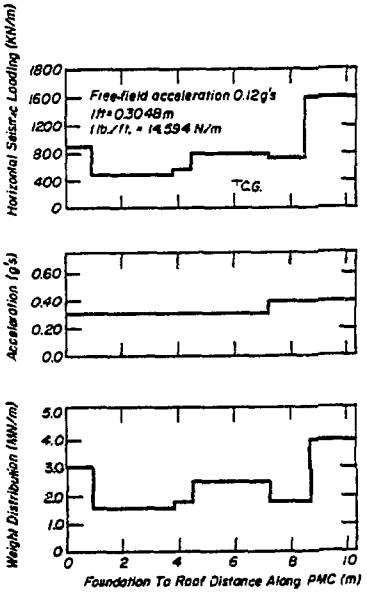

Fig. 47. PMC seismic loading in the N-S direction.

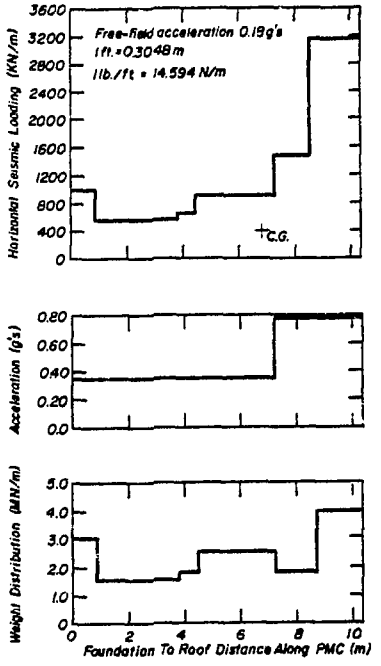

Fig. 48. PMC seismic loading in the N-S direction.

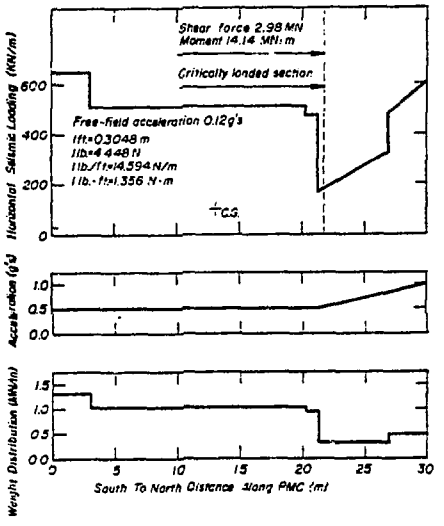

Fig. 49. PMC seismic loading in the E-W direction.

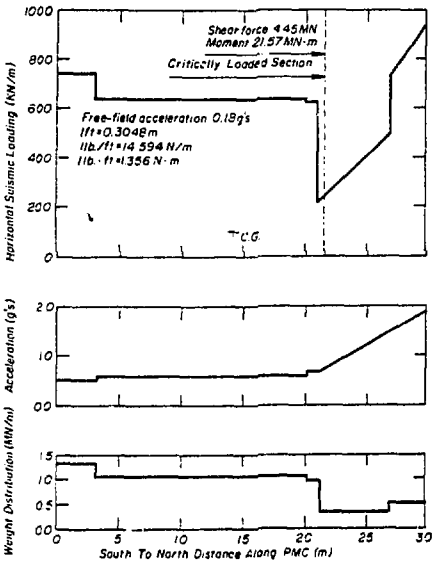

Fig. 50. PMC seismic loading in the E-W direction.

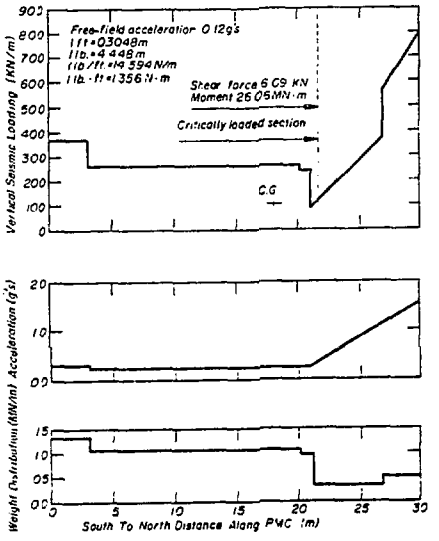

Fig. 51. PMC vertical seismic loading.

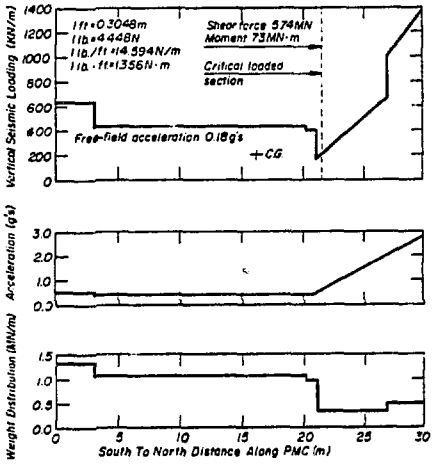

Fig. 52. PMC vertical seismic loading.

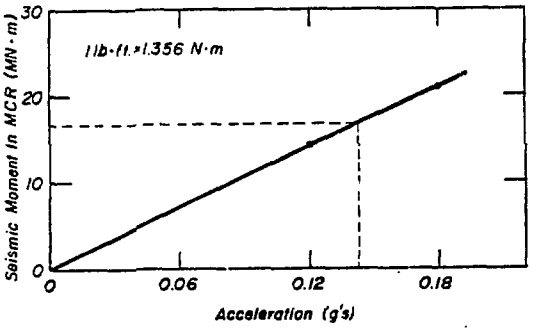

Fig. 53. MCR moment and acceleration relationship.

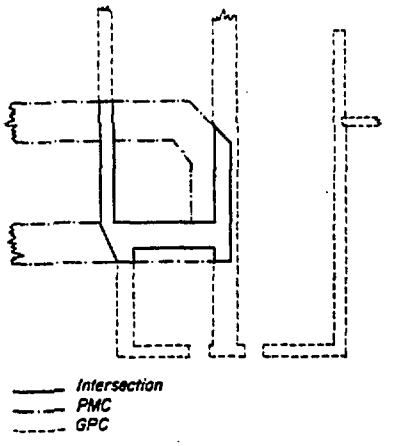

Fig. 54. PMC and GPC intersection.

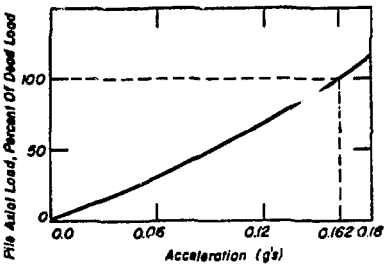

Fig. 55. Pile axial load vs acceleration relationship.

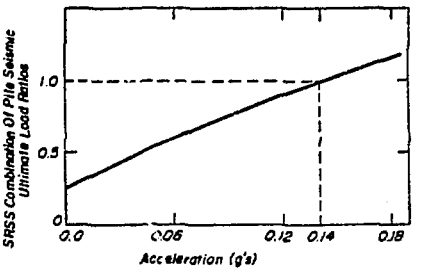

Fig. 56. SRSS pile seismic - ultimate load ratio - acceleration relationship.

APPENDIX A

SAMPLE CALCULATIONS

Below are listed the steps used to obtain the values indicated by the section titles.

I. CONCRETE PROPERTIES

A. Poisson's Ratio ν taken as 0.15.

B. The 28-day concrete strength was specified to be 17.24 MPa (2500 psi). The strength was increased 20% to 20.68 MPa (3000 psi) to account for aging effects.

C. Modulus of Elasticity Ec = 4730 $\sqrt{f'_c}$ = 21.52 GPa (3.12 x 10^6 psi).

D. Shear Modulus Gc = Ec/2(1 + ν) = 9.36 GPa (1.36 x 10^6 psi)

G_c = 196,000 kips/ft^2

II. EQUIVALENT CONCRETE SHEAR MODULI FOR SOIL-STRUCTURE MODELS

A. Reference: Drawing 2401-30-WBE-8001 in Ref. 11.

B. *Table showing cells and corresponding* ratios of wall cross-sectional area to total cell cross-sectional area at foundation level.

Cell	Area Ratio
CPC	0.41
XPC	0.37
LWC	0.24
GPC	0.50
EDR	0.26

C. The average ratio is 0.37.

D. The difference in form factors between the model and actual cross-sectional shapes reduces the average ratio. A value of 0.34 was selected.

E. (GA) model = (GA) plant

Gm (1) = (9360) (.34) = 3.18 GPa (66,641 kips/ft^2).

F. Used value of 3.20 GPa (67,500 kips/ft^2).

III. EQUIVALENT MODULI OF ELASTICITY AND SHEAR MODULI OF PILES IN SOIL-STRUCTURE MODELS

A. Modulus of Elasticity of Steel Es = 200 GPa (29 x 10^6 psi).

B. Flexural Equivalence for Lateral Motions.

C. Table of Pile Section Properties.

D. Idealized plant cross section at foundation level was taken to be 54.9 x 43.3 m (180 x 142 ft)

E. Pile cross sections in models were taken to be rectangular with unit depths and the selected widths from the table above.

F. Notation: ℓ is the selected model pile width and ℓ_o is 43.3 m for the N-S model and 54.9 m for the E-W model.

G. Poisson's Ratio for actual and model piles were taken to be the same.

H. Flexural Equivalence for Lateral Motions.

1. (EI)model = (EI)piles or (GI)m = (GI)p
2. G_m (1/12 $1_o \ell^3$) = (80.00 *GPa)(8.89* m^4)
3. G_m = 12(80.00)(8.89)/(43.3 $(0.762)^3$) - 445 MPa
4. G_m = 9300 kips/ft^2

I. Axial Shear Moduli for Vertical Motions.

1. (EA)model = (EA)piles or (GA)m = (GA)piles
2. G_m(1 ℓ_o) = (80.00 GPa)(0.825 m^2)
3. G_m = (80.00)(0.825) / (43.3)(0.762) = 2.00 GPa
4. G_m = 42,000 kips/ft^2

IV. MAXIMUM ROTATIONAL DEFORMATION IN NONMONOLITHIC CONNECTION BETWEEN THE CPC AND XPC

A. Section view of XPC shown in Fig. A-1.

B. From Fig. 55, the maximum pile load is 83% of the XPC dead load weight.

C. From Fig. A-2, the vertical acceleration response for a 0.14 g's earthquake is 0.44 g's.

D. The difference between the pile loads is 83-17 or 66%.

E. The differential pile stress is .66 (6.21 x 2) x 1.44 = 117.2 MPa (17,100 psi).

F. The pile lengths are taken as 18.3 m (60 ft) and are assumed to be end-bearing.

G. The rotational deformation at the roof elevation of the CPC is

$$\delta = \frac{\sigma L}{E} \cdot \frac{15.2}{7.0} = \frac{(117.2)\,(18.3)}{200.000} \frac{15.2}{7.0} =$$

23.3 mm (0.92 in.)

H. The connection detail is shown in Fig. A-3. The maximum allowable deflection in the direction of the rotational deflection is 25.4 x $\sqrt{2}$ or 36.0 mm (1.42 in.).

Property	Model	Model Pile Number 1	2	3	4
Number of Actual Piles	N-S	83	200	156	26
	E-W	70	172	172	51
Total Cross-Sectional Area, m^2 ($Sq.$ in.)	N-S	0.825 (1279)	2.013 (3120)	1.570 (2434)	0.262 (406)
	E-W	0.704 (1092)	1.731 (2683)	1.731 (2683)	0.514 (796)
Total Moment of Inertia* m^4 ($in.^4$)	N-S	8.89 (21361)	21.69 (52100)	16.92 (40640)	2.82 (6770)
	E-W	7.59 (18235)	18.65 (44806)	18.65 (44806)	5.47 (13152)
Selected model pile widths m (ft)	N-S	0.762 (2.5)	0.914 (3.0)	0.914 (3.0)	0.457 (1.5)
	E-W	0.610 (2.0)	0.914 (3.0)	0.914 (3.0)	0.610 (2.0)

*Total obtained by (1/2 N) I_y + (1/2 N) I_x, where N is the number of actual piles, I_x is the moment of inertia about the x-axis of the pile, and I_y is the moment of inertia about the pile y-axis.

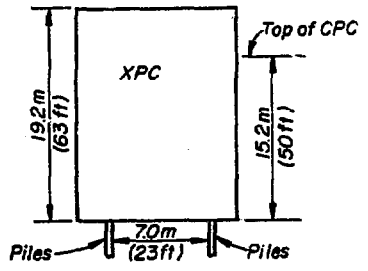

Fig. A.1. Section view of XPC.

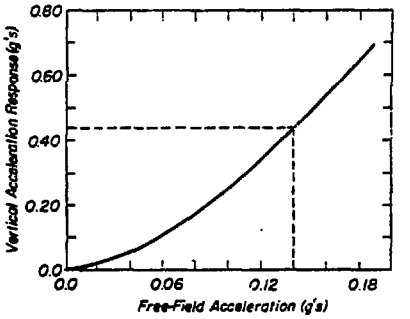

Fig. A.2. Vertical acceleration response vs free-field acceleration.

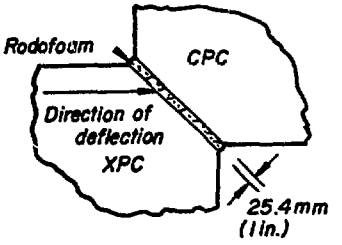

Fig. A.3. Interface detail between the CPC and XPC.

APPENDIX B

THE TEN PERCENT METHOD FOR CONTINUING MODAL RESPONSES

Notation:

$S_d(\omega)$ - the displacement response spectrum

$\{U_i\}$ - maximum modal response for the i^{th} mode

$\{\phi_i\}$ - eigenvector for i^{th} mode

$\{M_i\}$ - structural mass matrix

$S_{dx}(\omega_i)$, $S_{dx}(\omega_i)$, $S_{dz}(\omega_i)$ - spectral displacements for frequency ω_i in the x-, y-, and, z-directions

The maximum modal response for the i^{th} mode is given by

$$\{U_i\} = \{\phi_i\}|\{\phi_i\}^T \{M_i\}|S_{dx}(\omega_i)$$
$$+ \{\phi_i\}|\{\phi_i\}^T \{M_i\}|S_{dy}(\omega_i)$$
$$+ \{\phi_i\}|\{\phi_i\}^T \{M_i\}|S_{dz}(\omega_i)$$

where

$|\{\phi_i\}^T \{M_i\}|$ is defined as the participation factor.

The displacement in the x direction at node n is given by

$$U_{xn} = \left[\sum_{k=1}^{N} U^2_{xnk} + 2\Sigma|U_{xni}\, U_{xnj}|\right]^{1/2} \qquad i \neq j$$

where

N is the total number of modes considered and the second sum is carried out over only closely spaced modes.

Closely spaced modes are defined as

$$\frac{\omega_j - \omega_i}{\omega_i} \leq 0.1 \qquad \text{and } 1 \leq i \leq j \leq N.$$